UC Irvine
UC Irvine Previously Published Works

Title

Physical properties of EuPtIn4 intermetallic antiferromagnet

Permalink

https://escholarship.org/uc/item/60b4q2fx

Authors

Rosa, PFS
de Jesus, CBR
Fisk, Z
et al.

Publication Date

2014-12-01

DOI

10.1016/j.jmmm.2014.07.001

Copyright Information

Peer reviewed

Physical properties of EuPtIn$_4$ intermetallic antiferromagnet

P.F.S. Rosa [a,b,*], C.B.R. de Jesus [b], Z. Fisk [a], P.G. Pagliuso [b]

[a] University of California, Irvine, California 92697-4574, USA
[b] Instituto de Física "Gleb Wataghin", UNICAMP, Campinas, SP 13083-859, Brazil

ARTICLE INFO

ABSTRACT

We report the physical properties of EuPtIn$_4$ single crystalline platelets grown by the In-flux technique. This compound crystallizes in the orthorhombic Cmcm structure with lattice parameters $a = 4.542(1)$ Å, $b = 16.955(2)$ Å and $c = 7.389(1)$ Å. Measurements of magnetic susceptibility, heat capacity, electrical resistivity, and electron spin resonance (ESR) reveal that EuPtIn$_4$ is a metallic Curie–Weiss paramagnet at high temperatures with an effective moment of $\mu_{eff} \approx 7.8(1)$ μ_B due to divalent Eu ions. At low temperatures, antiferromagnetic (AFM) ordering is observed at $T_N = 13.3$ K followed by a successive anomaly at $T^* = 12.6$ K. In addition, within the magnetic state, a spin-flop transition is observed with $H_c \sim 2.5$ T at $T = 1.8$ K when the magnetic field is applied along the ac-plane. In the paramagnetic state, a single divalent Eu^{2+} Dysonian ESR line with a Korringa relaxation rate of $b = 4.1(2)$ Oe/K is observed. Interestingly, even at high temperatures, both ESR linewidth and electrical resistivity reveal a similar anisotropy. We discuss a possible common microscopic origin for the observed anisotropy in these physical quantities likely associated with an anisotropic magnetic interaction between Eu^{2+} $4f$ electrons mediated by conduction electrons.

1. Introduction

Low-dimensional rare-earth based intermetallic compounds exhibit a variety of interesting phenomena including Ruderman–Kittel–Kasuya–Yoshida (RKKY) magnetic interaction, heavy fermion (HF) behavior, unconventional superconductivity, crystalline electrical field (CEF) and Fermi surface (FS) effects [1,2]. In order to systematically explore the interplay between such versatile physical properties in structurally related series, it is highly desirable to separate the role of each interaction in determining the behavior of the system. For instance, the study of isostructural magnetic analogs have been often employed to elucidate the role of RKKY interactions and CEF effects in the evolution of the magnetic properties in $R_m M_n In_{3m+2n}$ (R=rare-earth; M=Rh, Ir; $m = 0, 1$; $n = 1, 2$) series [3,4]. In particular, Gd^{3+}- and Eu^{2+}-based members are usually taken as reference compounds due to their S-state ($S = 7/2$, $L = 0$) ground state. As such, CEF effects are higher order effects and their magnetic properties purely reflect the details of RKKY interaction and FS effects.

Among the Indium-rich compounds, several polycrystalline members of the series RM In$_4$ (114 system; R=e.g. Ca, Eu, Yb, Ce; M=e.g. Ni, Pd, Au) have been reported to adopt the orthorhombic YNiAl$_4$-type structure which contains complex [PtIn$_4$] polyanionic

networks with rare-earth atoms filling distorted hexagonal channels (Fig. 1a) [5–11]. Interestingly, the clear elongation of the b-axis indicates the possibility of a 2D Brillouin zone with cylindrical Fermi surfaces along the b direction. In particular, although the member CeNiIn$_4$ has been reported to display most likely a three-dimensional electronic state [14], the promising features of this series of compounds have not been extensively explored yet, particularly for single crystalline samples [12,14–16]. In order to test the above hypothesis in new members of this series, we here report the synthesis of EuPtIn$_4$ single crystals and their physical properties by means of electrical resistivity, magnetic susceptibility, specific heat and electron spin resonance (ESR) measurements. The field-dependent magnetic susceptibility shows an AFM ordering at $T_N = 13.3$ K followed by a successive transition at $T^* = 12.8$ K. Both electrical resistivity and ESR linewidth are found to be anisotropic even at high temperatures, suggesting the presence of an anisotropic magnetic interaction between the Eu^{2+} $4f$ electrons mediated by conduction electrons (ce). Such anisotropy is possibly caused by the low dimensionality of [PtIn$_4$] polyanionic networks surrounding the Eu^{2+} ions.

2. Experimental details

Single crystalline samples of EuPtIn$_4$ were grown using flux technique with starting composition Eu:Pt:In=1:1:25. The mixture was placed in an alumina crucible and sealed in a quartz tube

* Corresponding author at: University of California, Irvine, California 92697-4574, USA.
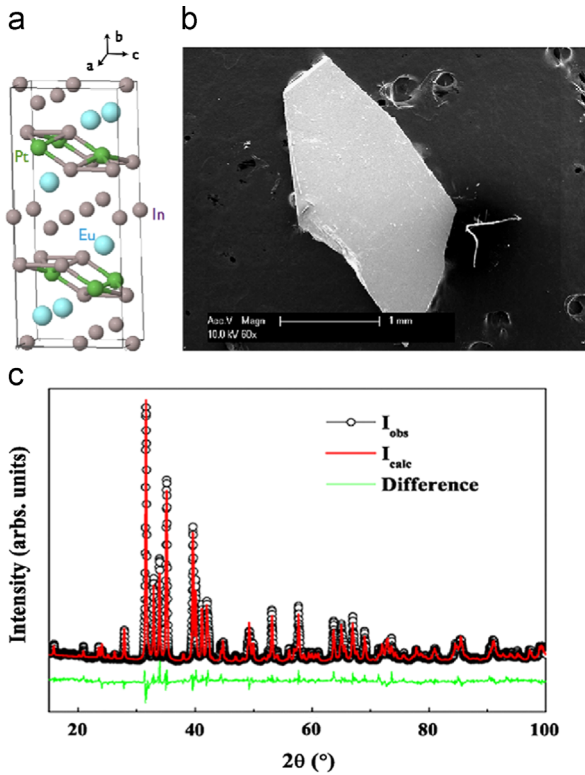 E-mail address: pfsrosa@uci.edu (P.F.S. Rosa).

Fig. 1. a) Orthorhombic crystal structure of EuPtIn$_4$ (space group Cmcm). (b) Scanning electron microscope (FE-SEM) image of as-grown EuPtIn$_4$ single crystal. (c) X-ray powder pattern and Rietveld fit ($R_{wp} = 13.6\%$) of EuPtIn$_4$ at 300 K.

under vacuum. The sealed tube was heated up to 1100 °C for 2 h, cooled down to 800 °C at 20 °C/h and then cooled down to 350 °C at 10 °C/h. The flux was then removed by centrifugation and the obtained shiny platelet crystals are stable in air and have typical dimensions of 1 mm × 1 mm × 0.1 mm, as shown in Fig. 1b. Phase purity was checked by X-ray powder diffraction using a Rigaku diffractometer (Cu–Kα radiation). Fig. 1c shows the pattern of EuPtIn$_4$, which could be completely fitted with a single phase. Rietveld refinements of EuPtIn$_4$ ($R_{wp} = 13.6\%$) yield lattice parameters $a = 4.542(1)$ Å, $b = 16.955(2)$ Å and $c = 7.389(1)$ Å. Specific heat measurements were performed in a Quantum Design PPMS small-mass calorimeter that employs a quasiadiabatic thermal relaxation technique. The electrical resistivity was measured using a standard four-probe method also in the Quantum Design PPMS. The magnetization was measured using a VSM superconducting quantum interference device (SQUID) magnetometer (Quantum Design). ESR measurements were performed in a BRUKER spectrometer equipped with a continuous He gas-flow cryostat. X-Band ($\nu \sim 9$ GHz) frequency was used in the temperature region 4.2 K < T < 300 K.

3. Results and discussion

The macroscopic physical properties of EuPtIn$_4$ single crystals are presented in Fig. 2. Panel (a) displays the zero-field electrical resistivity in-plane, ρ_{ac} (T), and along the b-axis, ρ_b (T), as a function of temperature. A weakly anisotropic metallic behavior is observed in the paramagnetic regime followed by a clear peak at $T_N = 13.3$ K. Residual resistivity (ρ_0) and residual resistivity ratio (RRR) values of $\rho(T)$ are $0.1 - 0.5$ $\mu\Omega$ cm and ~ 70, respectively, indicating good crystallinity of our samples. However, the magnetoresistance (MR $= \Delta\rho/\rho = \rho(H) - \rho(H=0)/\rho(H=0)$) at $T = 2$ K is

linear with magnetic field and no quantum oscillations have been found up to 14 T (inset of Fig. 2a).

Fig. 2b shows the magnetic susceptibility as a function of temperature for magnetic field of H = 1 kOe applied parallel and perpendicular to the ac-plane of the sample. $\chi(T)$ shows an isotropic Curie–Weiss (CW) behavior at high-T followed by an AFM transition at $T_N = 13.3$ K. The sharp decrease of $\chi(T)$ below T_N for H||ac-plane suggests that the ac plane is the plane of easy magnetization. From the CW magnetic susceptibility fits for $T > 10T_N$ (solid lines in Fig. 2b) we obtained for both directions a CW temperature of $\theta_{CW} \approx -15(1)$ K and an effective moment of $\mu_{eff} \approx 7.8(1)$ μ_B for Eu^{2+} in EuPtIn$_4$, which is in good agreement with the theoretical value (7.94 μ_B). Isothermal magnetization curves as a function of the applied magnetic field at 1.8 K are shown in the inset of Fig. 2b. On one hand, the magnetization increases linearly with field when H||b-axis, reaching an effective moment of 2.5 μ_B at 7 T, yet below the full Eu^{2+} moment of 7 μ_B. On the other hand, when H||ac-plane, a spin-flop transition is clearly observed at $H_c \sim 2.5$ T, also suggesting that the ac-plane is the plane of easy magnetization.

The AFM transition can also be observed in lower panel (c) of Fig. 2, which shows the specific heat as a function of temperature. In addition, in this case it is possible to observe two close sharp peaks in C/T at $T_N = 13.3$ K and $T^* = 12.8$ K. The former corresponds to the onset of AFM order and its value is consistent with the magnetic susceptibility anomaly (see Fig. 2b). The second peak at $T^* = 12.8$ K is likely related to a change of the magnetic structure. X-ray magnetic diffraction will help us to confirm this scenario. The estimated magnetic entropy recovered at T_N roughly reaches the value of $R \ln 8$ expected for the whole Eu^{2+} $S = 7/2$ ion (left inset of Fig. 2c). This confirms the divalent state of Eu ions in EuPtIn$_4$, similar to EuNiIn$_4$ and EuAuIn$_4$ compounds [8]. Finally, both transitions are slightly shifted downwards with applied magnetic field (right inset of Fig. 2c).

Now we turn our attention to the microscopic properties of EuPtIn$_4$. In this regard, ESR is a highly sensitive technique to study spin dynamics and magnetic interactions and it often reveals details about the microscopic interaction J_{fs} between the 4f electrons and the ce and about the Eu^{2+}–Eu^{2+} magnetic correlations (see for instance references [18–20]). Fig. 3 shows the X-Band ($\nu = 9.4$ GHz) ESR spectra for both orientations measured at $T = 100$ K. In both cases we observe a single ESR Dysonian resonance (i.e., microwave skin-depth smaller than the sample size) which indicates that the Eu^{2+} ions in EuPtIn$_4$ are embedded in a metallic environment [17]. From the fitting of the resonances to the appropriate admixture of absorption and dispersion at $T = 100$ K, we obtain for H||ac-plane a g-value of g = 2.02(3) and linewidth of $\Delta H = 840(80)$ Oe. On the other hand, for H along the b-axis, g = 1.97(4) and $\Delta H = 1100(100)$ Oe. Interestingly, even at high temperatures, Eu^{2+} ESR linewidth is anisotropic, as shown in Fig. 3b. Taking a closer look to the anisotropy for both rotation axis, one recognizes the presence of an orthorhombic contribution likely related to crystalline electrical field (CEF) effects found for $S = 7/2$ ions in orthorhombic systems [22]. Thus, the Eu^{2+} ESR linewidth has a contribution from an exchange narrowed ΔH with a distribution of local fields caused by unresolved fine (CEF splitting) and perhaps hyperfine structure. Using the g-value of Eu^{2+} in insulators as 1.993(2) we extract an apparent small g-shift which is negative ($\Delta g < 0$) for H||b and positive ($\Delta g > 0$) for H||ac-plane [22]. This small effect may be an indicative of an anisotropic Eu^{2+}–Eu^{2+} magnetic coupling with ferromagnetic Eu^{2+}–Eu^{2+} interaction in the ac-plane and antiferromagnetic Eu^{2+}–Eu^{2+} interactions between the layers. However, we cannot rule out the contribution of demagnetization effects on this apparent g-anisotropy. In addition, there is a weak T-dependence of the g-values, which may suggest the presence of short range
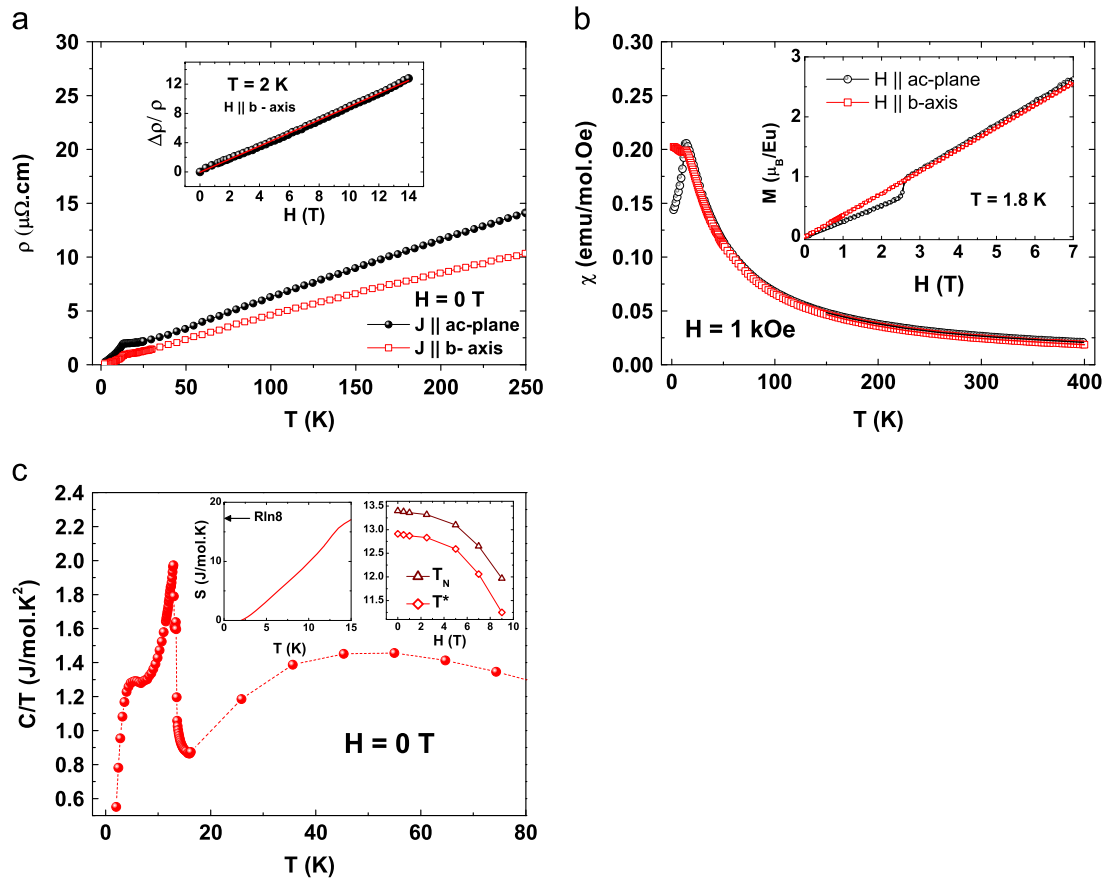
Fig. 2. Temperature dependence of macroscopic physical properties of EuPtIn$_4$ single crystals. (a) Electrical resistivity as a function of temperature for two current orientations. The inset shows the magnetoresistance for $H||$ b-axis at $T=2$ K. (b) Magnetic susceptibility with applied field $H=1$ kOe parallel to ac-plane and b-axis. (c) Temperature dependence of specific heat. The insets show the recovered entropy (left) and the suppression of T_N and T^* with applied field along the b-axis.

magnetic correlations yielding non-trivial local fields at the Eu^{2+} sites. Nevertheless, contributions from "*bottleneck*" and "*dynamic*" effects may be present [21]. ESR experiments in the dilute series Eu$_{1-x}$Sr$_x$PtIn$_4$ will help us to confirm this scenario and also to obtain further information about the relevant microscopic exchange interactions in this compound.

ΔH and g-value of EuPtIn$_4$ as a function of temperature for the X-Band are presented in Fig. 4a and b, respectively. An isotropic linear (Korringa) increase of ΔH with increasing T is observed for the Eu^{2+} ESR signal in the paramagnetic state. From linear fits to $\Delta H(T)$ (solid lines) for $T > 100$ K, we extracted the Korringa rate $b \equiv \Delta H/\Delta T = 4.1(2)$ Oe/K. As the temperature is further decreased, the ESR ΔH starts to broaden as a consequence of the development of short range magnetic correlations. At the same temperature region, the g-factor slightly increases, also suggesting the presence of a weak dominant ferromagnetic component. Finally, below T_N the resonance cannot be detected, likely due to the presence of antiferromagnetic collective modes which broaden the ESR line.

To further explore the microscopic origin of the Eu^{2+} ESR ΔH anisotropy we have performed detailed electrical resistivity experiments in both paramagnetic and ordered regimes. Fig. 5a shows a comparison between the anisotropy in Eu^{2+} ESR ΔH and that in the electrical resistivity. Such comparison is important in this case because an anisotropic exchange interaction between the Eu^{2+} $4f$ electrons mediated by ce would result in similar angular dependence of both physical quantities. In fact, we observe that both properties display resemblant anisotropy, suggesting the presence of anisotropic magnetic scattering due to anisotropic short range magnetic correlations between Eu^{2+} ions. In addition, Fig. 5c shows

a subtle change of anisotropy in the antiferromagnetic state as compared to the paramagnetic one (Fig. 5b), in agreement with the above picture.

Note added: During initial submission of the paper, we became aware of a related work on EuPtIn$_4$ single crystals [13]. Apart from the distinct value of $T^* = 5$ K, the experimental results are in very good agreement with the present paper. We attribute this difference to a possible slight fluctuation of Indium stoichiometry in the EuPtIn$_4$ crystals, which would not necessarily influence their quality. For instance, in Ref. [13] the Eu:Pt:In ratio used is 1:1:16 for their single crystal growth. Even for our samples grown with ratio Eu:Pt:In of 1:1:25, Energy Dispersive Spectroscopy (EDS) elemental analysis provides an actual ratio of 1:1:3.7 in our single crystals. Furthermore, we would like to emphasize that our macroscopic and microscopic results combined provide strong evidence for the divalent state of Eu ions, suggesting that an intermediate valence of Eu ions is not realized in the studied compound [13].

4. Conclusion

Here we report the synthesis, macroscopic characterization and ESR experiments on single crystalline samples of EuPtIn$_4$. This compound crystallizes in a low-dimensional orthorhombic structure (space group Cmcm) and presents AFM ordering below $T_N = 13.3$ K. A spin-flop transition is observed at $H_c \sim 2.5$ T for magnetic fields applied along the ac-plane of easy magnetization. In the paramagnetic state, a single Eu^{2+} Dysonian ESR line with a Korringa-type relaxation is observed, indicating that Eu ions
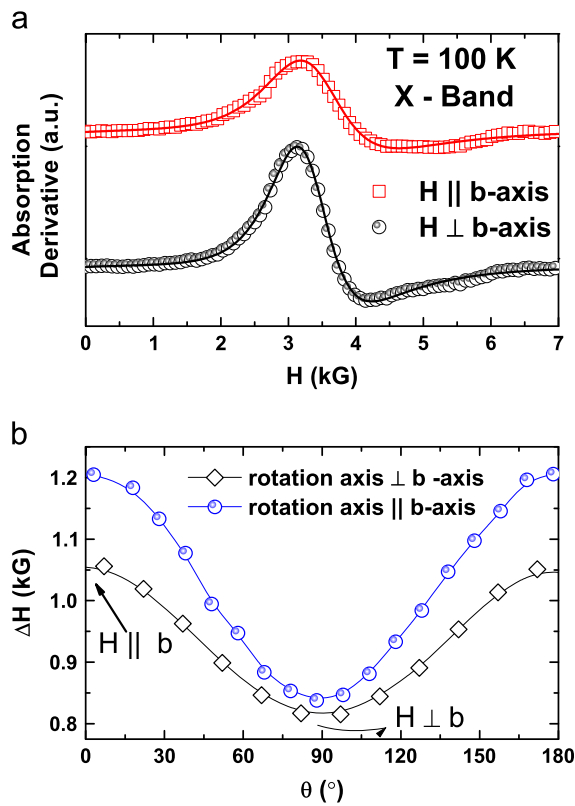
Fig. 3. (a) X-Band ($\sim$9.5 GHz) ESR spectra of EuPtIn$_4$ single crystals at $T=100$ K. (b) Angle dependence of ESR linewidth ΔH.
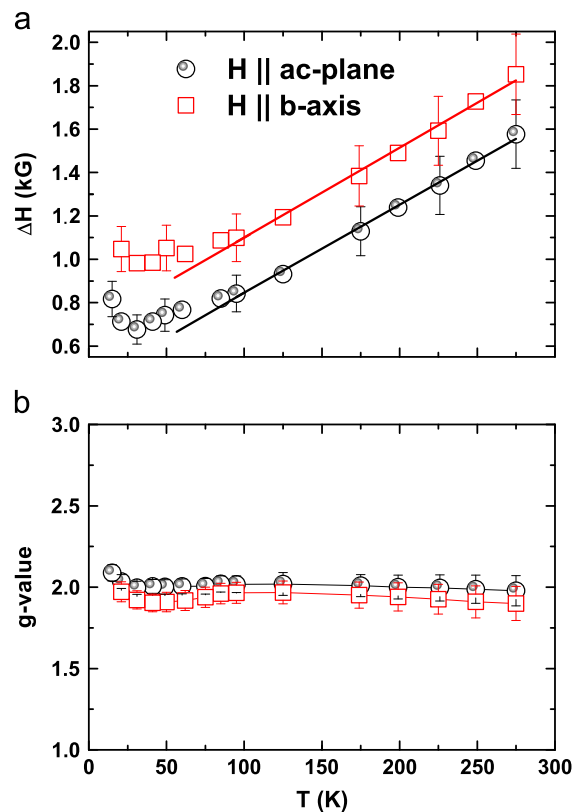

Fig. 4. Temperature dependence of Eu^{2+} ESR ΔH and g-factor in X-Band.
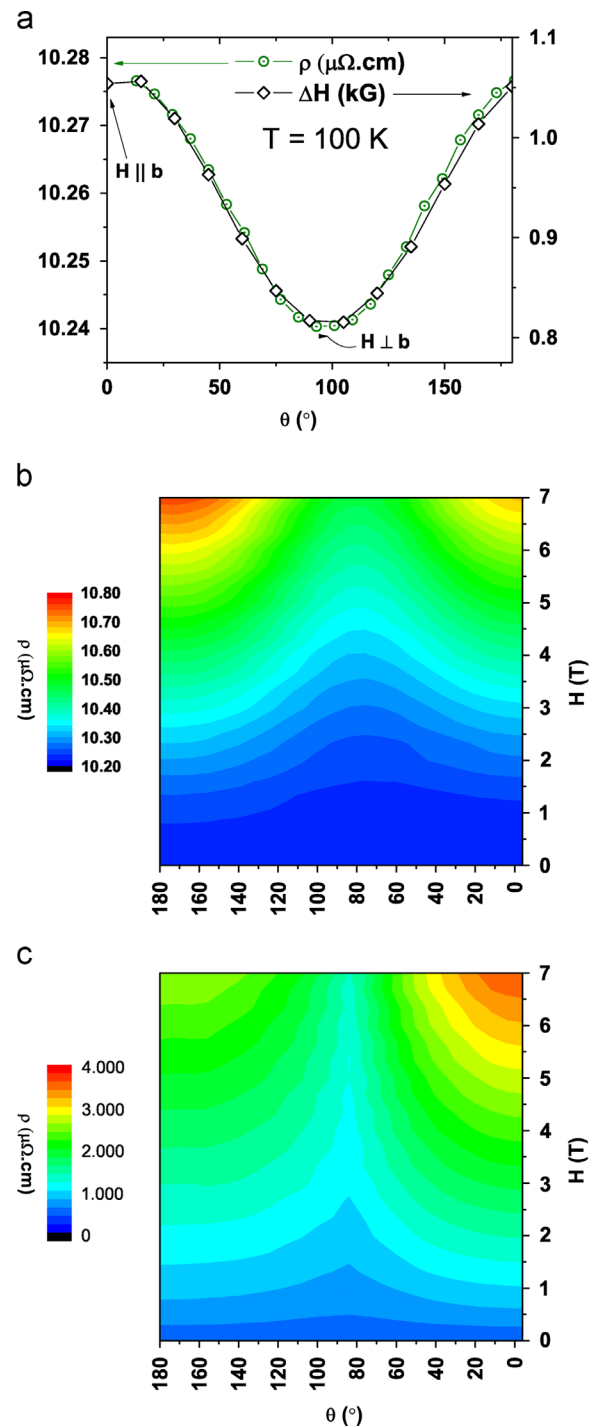

Fig. 5. (a) Angle dependence of electrical resistivity and ESR linewidth. Resistivity maps as a function of angle and magnetic field at (b) $T=100$ K and (c) $T=2$ K.

are divalent and experience a metallic environment in EuPtIn$_4$. The anisotropy of ESR linewidth and electrical resistivity at high T indicates the presence of both second order CEF effects and anisotropic exchange interaction between the Eu^{2+} 4f electrons mediated by ce. Ultimately, the presence of such an anisotropic electronic vicinity may arise from the [PtIn$_4$] polyanionic networks surrounding the Eu^{2+} ions.

Acknowledgments

References

[1] Z. Fisk, et al., Proc. Natl. Acad. Sci. USA 92 (1995) 6663.
[2] H.v. Löhneysen, et al., Rev. Mod. Phys. 79 (2007) 1015.
[3] P.G. Pagliuso, et al., Phys. Rev. B 63 (2001) 054426.
[4] E. Granado, et al., Phys. Rev. B 69 (2004) 144411.
[5] Y.M. Kalychak, et al., Sov. Phys. Crystallogr. 33 (1988) 602–603.
[6] R.-D. Hoffmann, R. Pottgen, Chem. Eur. J. 6 (2000) 600–607.
[7] R.-D. Hoffmann, R. Pottgen, V.I. Zaremba, U.M. Kalychak, Z. Naturforschung B 55 (2000) 834–840.
[8] R. Pottgen, R. Mollmann, B.D. Mosel, H. Eckert, J. Mater. Chem. 6 (1996) 801–805.
[9] R.J. Pottgen, Mater. Chem. 5 (1995) 769–772.
[10] M.D. Koterlin, B.S. Morokhivski, I.D. Shcherba, Ya.M. Kalychak, Solid State 41 (1999) 1759–1762.
[11] Y.V. Galadzhun, R. Pottgen, Z. Anorg. Allg. Chem. 625 (1999) 481–487.
[12] V.I. Zaremba, et al., Z. Anorg. Allg. Chem. 629 (2003) 1157–1161.
[13] P. Kushwaha, et al., Cryst. Growth Des. 14 (2014) 2747–2752.
[14] H. Shishido, et al., J. Phys. Soc. Jpn. 73 (3) (2004).
[15] S. Sarkar, et al., Cryst. Growth Des. 13 (2013) 4285.
[16] S.N. Nesterenko, A.I. Tursina, D.V. Shtepa, H. Noel, Y.D.J. Seropegin, Alloys Compd. 442 (2007) 93–95.
[17] F.J. Dyson, Phys. Rev. 98 (1955) 349.
[18] R.R. Urbano, et al., Phys. Rev. B 70 (2004) 140401(R).
[19] P.F.S. Rosa, et al., Phys. Rev. B 87 (2013) 224414.
[20] P.F.S. Rosa, et al., Phys. Rev. B 86 (2012) 094408.
[21] C. Rettori, et al., Phys. Rev. B 10 (1974) 1826.
[22] A. Abragam, B. Bleaney, Electron Paramagnetic Resonance of Transition Ions, Clarendon Press, Oxford, 1970.